Article:
Guan, S., Zhang, Y., Zhang, S. et al. (2026) Supramolecular near-infrared photocatalysts for efficient and oxygen-tolerant aqueous RAFT polymerization. Angewandte Chemie International Edition, 65 (28). e8665452. ISSN: 1433-7851

https://doi.org/10.1002/anie.8665452

Supramolecular Near-Infrared Photocatalysts for Efficient and Oxygen-Tolerant Aqueous RAFT Polymerization

Siyan Guan, [a] Yue-Yi Zhang, [c] Shudi Zhang, [a] Zhi-Yuan Zhang, [c] Steven P. Armes, [d] Chunju Li, [c]* and Zesheng An [a,b] *

[a] S. Guan, S. Zhang, Prof. Z. An
State Key Laboratory of Supramolecular Structure and Materials
College of Chemistry, Jilin University
Changchun 130012 (China)
E-mail: anzesheng@jlu.edu.cn

[b] Prof. Z. An
Key Laboratory for Molecular Enzymology and Engineering of Ministry of Education
School of Life Sciences, Jilin University
Changchun 130012 (China)

[c] Y. Zhang, Dr. Y.-Z. Zhang, Prof. C. Li
Academy of Interdisciplinary Studies on Intelligent Molecules
Tianjin Key Laboratory of Structure and Performance for Functional Molecules
College of Chemistry, Tianjin Normal University, Tianjin 300387 (China)
E-mail: cjli@shu.edu.cn

[d] Prof. S. P. Armes
School of Mathematical and Physical Sciences
University of Sheffield
Sheffield, South Yorkshire, S3 7HF, UK

Supporting information for this article is given via a link at the end of the document.

Abstract: Near-infrared (NIR) photocontrolled polymerization in aqueous media is promising for bioapplications. However, it typically suffers from low polymerization efficiency and requires high catalyst loadings due to the aggregated nature of the photocatalyst. Herein, we report a supramolecular strategy to overcome this limitation via host–guest complexation between an anionic photocatalyst and a cationic macrocycle. Spectroscopic and computational studies confirmed the formation of stable 1:1 host–guest complexes via synergistic electrostatic, π-π, and hydrophobic interactions. Supramolecular complexation effectively suppresses photocatalyst aggregation and significantly enhances oxygen tolerance and reaction kinetics, enabling high-throughput, open-to-air NIR-mediated reversible addition-fragmentation chain-transfer (RAFT) polymerizations to be conducted in aqueous media with excellent control over molecular weight and dispersity. High conversions and low dispersities were achieved even for polymerizations conducted through thick porcine tissue barriers, demonstrating excellent NIR penetration depth. This work provides a versatile supramolecular approach to enhancing photocatalyst performance, highlighting new avenues for precision polymer synthesis under biologically relevant conditions.

Introduction

Photocontrolled reversible deactivation radical polymerization (photo-RDRP) has emerged as a powerful strategy for the precision synthesis of advanced functional polymers, owing to its mild reaction conditions, excellent living character, and spatiotemporal control.[1] In particular, systems that integrate reversible addition-fragmentation chain transfer (RAFT) polymerization with various light activation pathways have proven to be exceptionally versatile and applicable to a wide range of monomers under diverse conditions.[2] However, most photocontrolled RAFT polymerizations typically rely on ultraviolet or visible light, which restricts their potential biological applications where deep tissue penetration and high biocompatibility are paramount.

Near-infrared (NIR) light is ideally suited to address these limitations owing to its longer wavelength and proven biocompatibility.[3] Consequently, the development of NIR photocontrolled radical polymerization has attracted considerable interest.[4] Photoinduced electron/energy transfer RAFT (PET-RAFT) is an extremely versatile approach that has attracted growing interest in precision polymer synthesis using a wide range of wavelengths, including

the NIR region.[5] The central challenge in this endeavor is the design of effective photocatalysts that can simultaneously deliver high polymerization rates, excellent control over the target molecular weight and dispersity, and good tolerance towards oxygen. Several NIR photocatalysts, including porphyrins,[5a, 6] phthalocyanines,[5c, 7] cyanines,[8] and methylene blue,[9] have been employed for this purpose. Nonetheless, such extensively conjugated compounds are typically prone to form aggregates in aqueous media, while resorting to organic co-solvents diminishes their suitability for biomedical applications. Although structural modifications can enhance water solubility, such approaches typically require laborious multi-step syntheses and purification.[7c] Therefore, developing simple, effective, and modular strategies to enable efficient, oxygen-tolerant NIR photocontrolled RAFT polymerization in aqueous media remains a significant challenge.

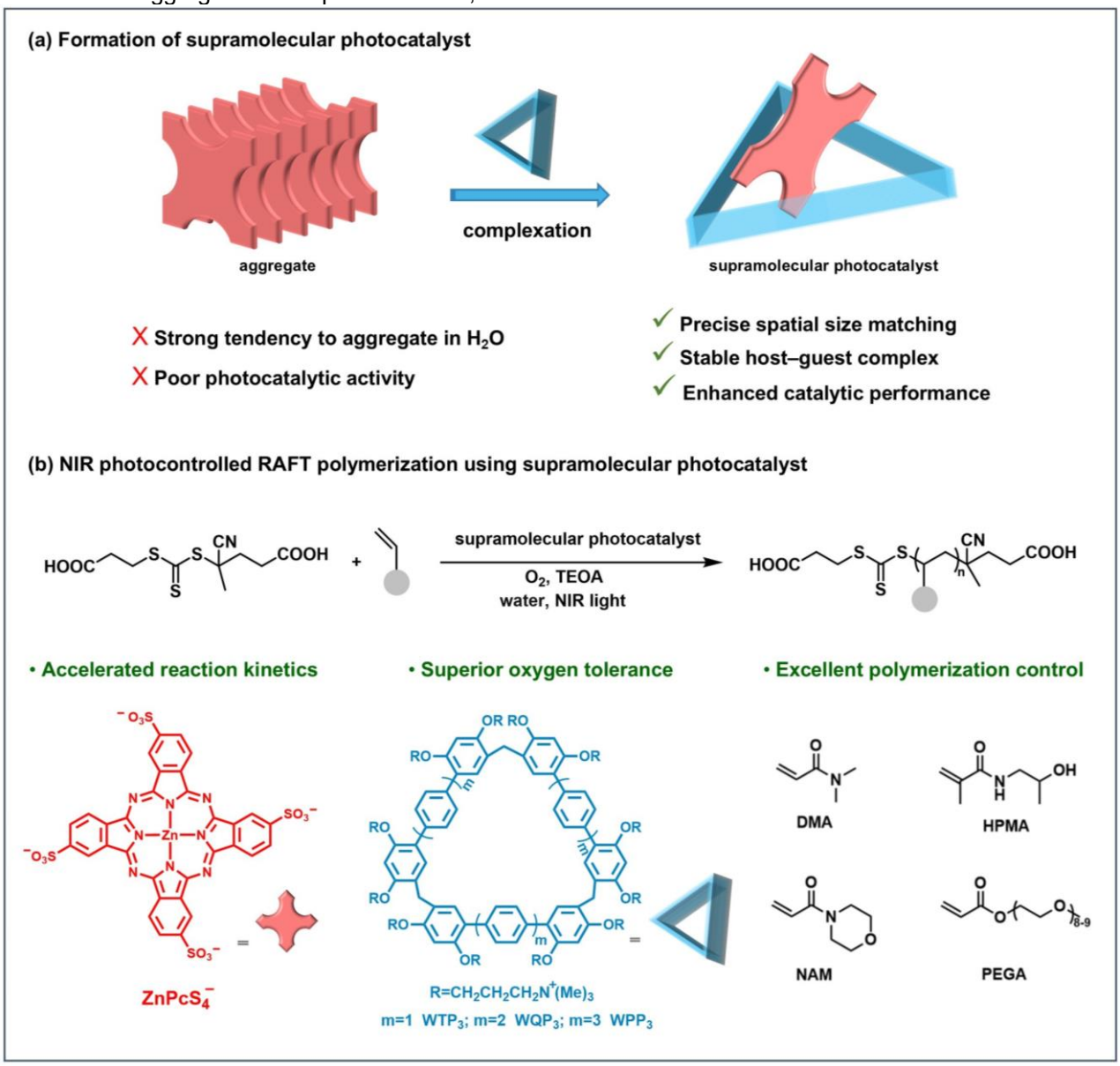

Scheme 1. (a) Schematic formation of a supramolecular NIR photocatalyst. Using a suitable macrocyclic host ensures that the photocatalyst forms a host–guest complex in aqueous solution, rather than aggregates. (b) NIR photocontrolled RAFT polymerization in aqueous media using such a supramolecular photocatalyst; chemical structures of the $ZnPcS_4^-$ photocatalyst, macrocyclic host molecules, and monomers used in this study.

In contrast to complex organic synthesis, supramolecular host–guest interactions offer a highly modular and versatile platform for constructing functional assemblies, with broad applications in organic transformations, biomedical therapy, cellular imaging, and dynamic materials.[10] Inspired by these advances, we hypothesized that host–guest chemistry could provide a straightforward and versatile method to construct water-soluble supramolecular NIR photocatalysts, thereby improving photocatalytic efficiency and enabling efficient, oxygen-tolerant photocontrolled RAFT polymerization in aqueous media (**Scheme 1**). In this study, we employ biphen[*3*]arenes as macrocyclic hosts with cavities of tunable size to

form complexes with photocatalysts such as zinc phthalocyanine tetrasulfonate ($ZnPcS_4^-$) or tetra(4-carboxyphenyl)porphyrin (TCPP). This supramolecular strategy enhances both oxygen tolerance and radical production efficiency, resulting in significantly accelerated polymerization kinetics while maintaining excellent control over aqueous polymerizations conducted under mild ambient conditions.

Results and Discussion

Formation of supramolecular photocatalyst biphen[*3*]arene–$ZnPcS_4^-$

$ZnPcS_4^-$ has been employed as a water-soluble photocatalyst to conduct NIR-mediated RAFT polymerizations in aqueous media owing to its strong NIR absorption and high triplet quantum yield.[5c] However, its tendency to aggregate in water significantly diminishes its catalytic performance.[11] We recently addressed this issue by constructing a supramolecular NIR photoenzyme, whereby complexation of $ZnPcS_4^-$ with glucose oxidase (GOx) spatially confines this photocatalyst, enabling access to ultrahigh molecular weights at catalyst loadings as low as 50 ppb.[12] Herein, we explore an alternative supramolecular approach using biphen[*3*]arene macrocycles, which were chosen for their structural diversity, modularity, and multifunctionality.[13] The cavity size of these macrocycles can be tuned by varying the biphenylene length,[14] enabling them to form host–guest complexes with targets ranging from small molecules[15] to complex macromolecules.[16] Three extended biphen[*3*]arene derivatives, each functionalized with twelve quaternary ammonium groups, were selected to investigate their complexation with $ZnPcS_4^-$ through host–guest and electrostatic interactions.

The catalytic efficiency of such biphen[*3*]arene–$ZnPcS_4^-$ complexes was first evaluated for the RAFT polymerization of *N*, *N*-dimethylacrylamide (DMA) using 4-((((2-carboxyethyl)thio)carbonothioyl)thio)-4-cyanopentanoic acid (CTPA) as a chain transfer agent (CTA) in the presence of air under NIR light irradiation (λ_{max} = 738 nm; I = 60 mW cm^{-2}). The photocatalyst is proposed to play dual roles in such polymerizations. More specifically, triplet oxygen ($^3O_2$) photosensitization by $ZnPcS_4^-$ generates singlet oxygen ($^1O_2$),[5c, 17] which is subsequently reduced by triethanolamine (TEOA) to produce superoxide radical anion. This latter species undergoes dismutation to produce hydrogen peroxide, which is then photosensitized by $ZnPcS_4^-$ to generate hydroxyl radicals, thereby initiating RAFT polymerization.[5c] Although all three biphen[*3*]arenes led to higher monomer conversions relative to the use of $ZnPcS_4^-$ alone, WQP_3 produced the fastest polymerization (**Table S1**; **Figure S2**). UV–visible spectroscopy studies revealed a large red shift in the Q-band for each complex, with the largest absorbance enhancement observed for WQP_3 (**Figure S3**). This suggests that WQP_3 forms the most stable host–guest complex with $ZnPcS_4^-$, presumably because its cavity size is well suited for hydrophobic, π-π, and electrostatic interactions with $ZnPcS_4^-$.[15c, 18] Based on these observations, WQP_3 was identified as the optimal host for further detailed investigation. The formation of the WQP_3–$ZnPcS_4^-$ complex was characterized by a combination of spectroscopic and computational studies. Titration of WQP_3 into a $ZnPcS_4^-$ solution induced significant spectral changes for the photocatalyst: its λ_{max} was red-shifted from 635 nm to 684 nm with substantially enhanced absorbance (**Figure 1a**). Analysis of the change in absorbance at 684 nm versus the WQP_3/$ZnPcS_4^-$ molar ratio indicated the formation of a host–guest complex with a 1:1 binding stoichiometry (**Figure 1b**). Conversely, titration of $ZnPcS_4^-$ into a WQP_3 solution gradually quenched the fluorescence of the macrocycle, yielding an association constant (K_a) of 3.18×10^7 M^{-1} (**Figure 1c-d**)[19] and suggesting the formation of a relatively stable complex. Electrospray ionization mass spectrometry (ESI-MS) studies indicated an m/z peak corresponding to the 1:1 complex with a net charge of +8 (12 positive charges from WQP_3 plus 4 negative charges from $ZnPcS_4^-$) (**Figure 1e**), which provides good evidence for the formation of a stable stoichiometric complex. Gaussian-accelerated molecular dynamics (GaMD) simulations[20] provided optimized conformations of the WQP_3–$ZnPcS_4^-$ complex (**Figure 1f**). WQP_3 displays a cavity defined by the three *p*-quaterphenylene sides connected by methylene bridges at the *meta*-positions of the terminal benzene rings, with the twelve quaternary ammonium cations distributed around the main scaffold so as to minimize charge repulsion. The twisted $ZnPcS_4^-$ plane faces one side of the WQP_3; one of its four isoindole units is fully incorporated into the cavity, the two perpendicular isoindole units are located

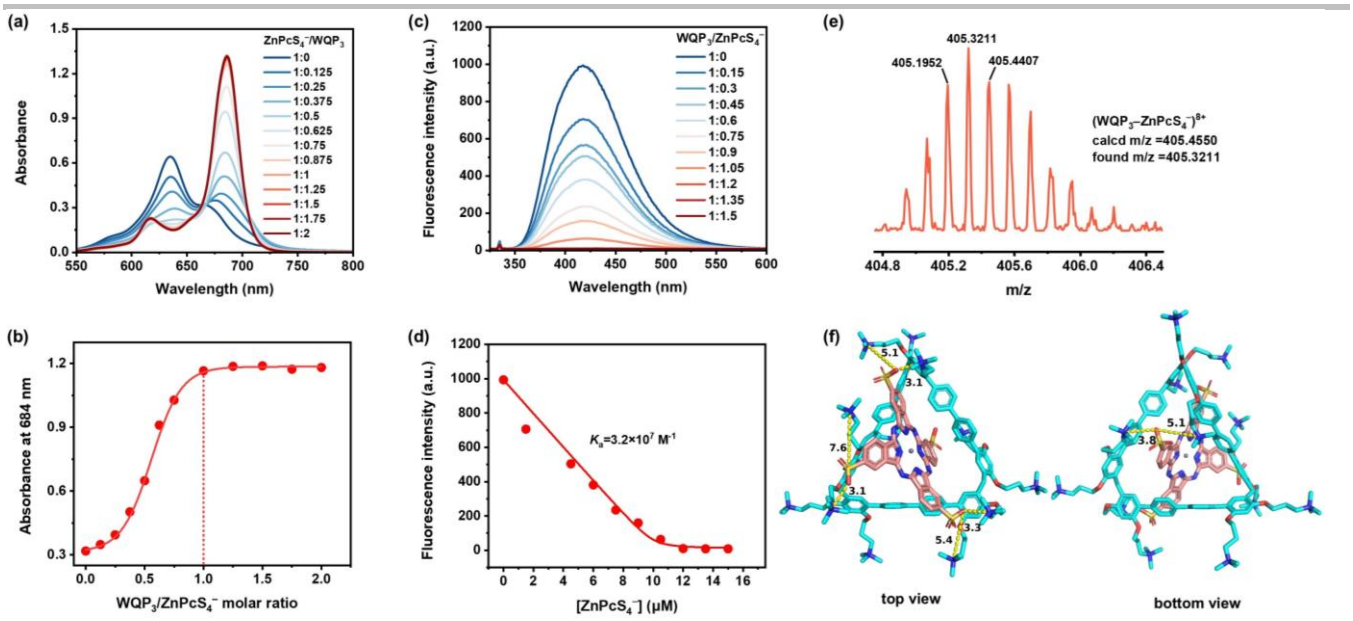

Figure 1. Characterization of the host–guest complexation between WQP_3 and $ZnPcS_4^-$. (a) UV–visible absorption spectroscopy monitoring of WQP_3 titration into a 10 μM $ZnPcS_4^-$ solution. (b) Plots of absorbance at 684 nm versus $WQP_3/ZnPcS_4^-$ molar ratio. (c) Fluorescence spectroscopy monitoring of $ZnPcS_4^-$ titration into a 10 μM WQP_3 solution (λ_{ex} = 335 nm slit width: 5 nm, 5 nm). (d) Nonlinear least-square analysis to determine the association constant (K_a). (e) ESI-MS spectrum recorded for the WQP_3–$ZnPcS_4^-$ complex. (f) Optimized molecular geometry indicated by GaMD simulation

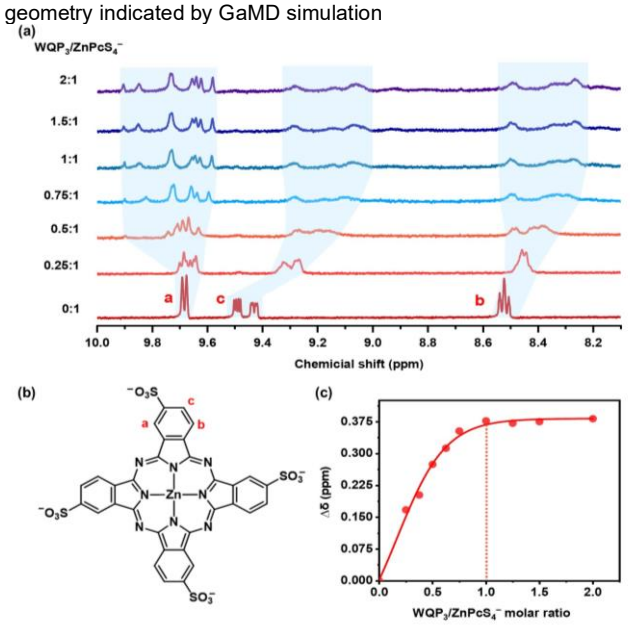

Figure 2. ^1H NMR spectroscopy (500 MHz, 25 °C, DMSO-d_6, number of scans: 128) studies of the titration of WQP_3 into $ZnPcS_4^-$ (0.40 mM). (a) Evolution of $ZnPcS_4^-$ spectra on increasing the $WQP_3/ZnPcS_4^-$ molar ratio. (b) $ZnPcS_4^-$ chemical structure with labeled protons. (c) Plot of the change in chemical shift (Δδ) for the $ZnPcS_4^-$ proton *b* (the most upfield split) versus $WQP_3/ZnPcS_4^-$ molar ratio. (Under the NMR measurement concentration, $ZnPcS_4^-$ undergoes strong aggregation in D_2O. This results in a drastic reduction in proton relaxation times, which prevents observation of the proton signals. In contrast, DMSO-d_6 can more effectively disrupt the π–π stacking interaction).

just above two *p*-quaterphenylene sides, and the fourth isoindole unit points away from the host molecule. Each of the four anionic sulfonate groups of $ZnPcS_4^-$ has a strong electrostatic interaction with the two nearest ammonium cations, as evidenced by their relatively short distances. This optimized geometry reveals that hydrophobic, π-π, and electrostatic interactions synergistically drive the formation of a stable host–guest complex. We further investigated their complexation behavior via 1D and 2D ^1H NMR spectroscopy. Titration of WQP_3 into $ZnPcS_4^-$ induced clear splitting patterns for the three proton signals of $ZnPcS_4^-$ due to their differing microenvironments (**Figure 2a**). The photocatalyst's protons *b* and *c* and the macrocycle's skeleton protons both shifted upfield while simultaneously becoming broader (**Figure S12**) owing to the mutual shielding effect for face-to-face stacking between the aromatic rings of the host and guest.[21] 2D nuclear overhauser effect spectroscopy (NOESY) also indicated the close spatial proximity between the skeleton protons of WQP_3 and those of $ZnPcS_4^-$ (**Figure S13**), strongly supporting the inclusion of $ZnPcS_4^-$ into the cavity of WQP_3. However, proton a assigned to $ZnPcS_4^-$ exhibited a more complex pattern with both upfield and downfield splits. While the upfield shift is attributed to a cavity shielding effect, the downfield signal is primarily due to strong electrostatic interactions of the anionic sulfonate with the ammonium cation and intramolecular hydrogen bonding interactions. The combination of multiple deshielding and shielding effects ultimately leads to the complex splitting pattern of proton a. A spectrum acquired on a 600 MHz NMR instrument at 80 °C provided a 1:2:1 integral ratio for each set of proton signals of $ZnPcS_4^-$ (**Figure S14**), corroborating the host–guest geometry indicated by GaMD simulation: one isoindole unit of $ZnPcS_4^-$ inserts deeply into the WQP_3 cavity and experiences the strongest shielding effect, two isoindole units are positioned near the cavity with moderate shielding, and the fourth isoindole unit remains largely outside the cavity with minimal shielding. Quantitative analysis of the changes in chemical shift for the $ZnPcS_4^-$ protons indicated complexation at a 1:1 host–guest molar ratio

(**Figure 2c)**, which is consistent with the visible spectroscopy titration data.

NIR photocontrolled polymerization mediated by supramolecular photocatalyst

After a comprehensive understanding of WQP_3–$ZnPcS_4^-$ complexation, we compared the DMA polymerization kinetics in a sealed microtiter plate without deoxygenation using $ZnPcS_4^-$ alone and the WQP_3–$ZnPcS_4^-$ complex under NIR light irradiation (λ_{max} = 738 nm; I = 60 mW cm^{-2}). When targeting a degree of polymerization (DP) of 500, the complex ($WQP_3/ZnPcS_4^-$ molar ratio = 1:1) produced a significantly higher conversion compared to $ZnPcS_4^-$ alone (79% vs. 53%) within 12 h (**Table S2**). Although both systems exhibited excellent pseudo-first-order kinetics, a significantly faster polymerization rate was observed for the 1:1 complex, with a more than two-fold increase in the apparent rate constant (k_p^{app}: 0.137 h^{-1} vs 0.064 h^{-1}) (**Figure 3**). This confirms the higher catalytic efficiency of the supramolecular photocatalyst. Moreover, gel permeation chromatography analysis using a multi-angle laser light scattering detector (GPC-MALLS) revealed that the experimental number-average molecular weight (M_n) closely matched the theoretical values, as well as narrow, monomodal molecular weight distributions ($Đ$ = 1.05). These results clearly demonstrate that the supramolecular photocatalyst can indeed accelerate the polymerization kinetics while maintaining excellent control.

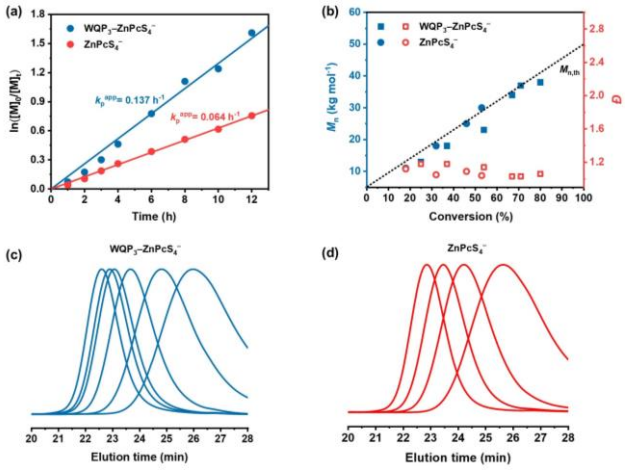

Figure 3. Kinetic studies for DMA polymerizations obtained using $ZnPcS_4^-$ and WQP_3–$ZnPcS_4^-$. (a) Pseudo-first-order plots of $\ln([M]_0/[M]_t)$ versus time. (b) Plots of molecular weight and dispersity versus conversion. (c-d) Corresponding GPC traces recorded for the PDMA homopolymers. Polymerization conditions: [DMA]/[CTPA] = 500, [TEOA] = 0.19 M, [$ZnPcS_4^-$] = 0.24 mM (50 ppm relative to monomer), [WQP_3] = 0.24 mM, monomer content = 50% v/v, solution volume = 260 µL, air volume = 80 µL, 28 °C, NIR light (λ_{max} = 738 nm; I = 60 mW cm^{-2}).

Having proven that the supramolecular photocatalyst can enhance catalytic efficiency and accelerate polymerization kinetics, we sought to further optimize this platform for high-throughput experiments.[22] This strategy employs oxygen to generate hydroxyl radicals[1j, 23] and the inherent oxygen tolerance can be utilized for benchtop screening of reaction parameters within microvolumes. Thus, the headspace air volume, concentrations of TEOA, $ZnPcS_4^-$ and WQP_3 were systematically varied to understand their effects on the polymerization rate and degree of control (**Figures S18–S19**, **Tables S4–S5**). Each of these reaction parameters was positively correlated with monomer conversion until a plateau value was reached. Moreover, increasing the $WQP_3/ZnPcS_4^-$ molar ratio beyond 1:1 can drive the complexation equilibrium, further enhancing the polymerization rate. To maximize this effect while minimizing materials consumption, the following conditions were determined to be optimal and used for further studies: headspace volume = 170 µL, TEOA concentration = 0.19 M, $ZnPcS_4^-$ loading = 50 ppm (relative to monomer), $WQP_3/ZnPcS_4^-$ molar ratio = 2:1.

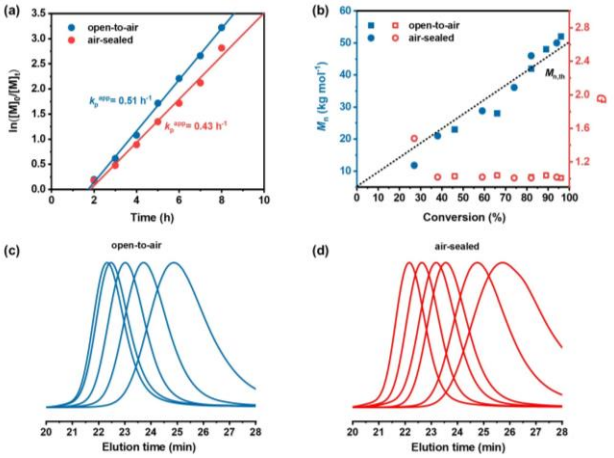

Figure 4. Kinetic studies for the DMA polymerizations conducted under sealed condition (without deoxygenation) and open-to-air condition using WQP_3–$ZnPcS_4^-$. (a) Pseudo-first-order plots of $\ln([M]_0/[M]_t)$ versus time. (b) Plots of molecular weight and dispersity versus conversion. (c-d) GPC traces recorded for the PDMA homopolymers obtained during the corresponding polymerization process. Polymerization conditions: [DMA]/[CTPA] = 500, [TEOA] = 0.19 M, [$ZnPcS_4^-$] = 0.24 mM (50 ppm relative to monomer), [WQP_3] = 0.48 mM, monomer content = 50% v/v, solution volume = 170 µL, air volume = 170 µL, 28 °C, NIR light (λ_{max} = 738 nm; I = 60 mW cm^{-2}).

Kinetic studies were then conducted under optimized conditions without deoxygenation in both sealed and open systems (**Figure 4**). When using the supramolecular catalyst, both systems achieved near-quantitative conversion within 8 h, in contrast to the 34% conversion observed with $ZnPcS_4^-$ alone (**Table S7, entry 6**), thus confirming the significantly enhanced polymerization efficiency under optimized conditions. Despite an induction period (~1.8 h) due to the presence of a relatively large air volume (air/solution = 1:1 v/v), both systems exhibited excellent pseudo-first-order kinetics, indicating a constant radical concentration during the polymerization. A higher polymerization rate was observed for the open-to-air system compared to the sealed system (k_p^{app}: 0.51 h^{-1} vs. 0.43 h^{-1}). This is

because more oxygen is available for the generation of hydroxyl radicals in the former case. Furthermore, both systems provided excellent polymerization control with closely matched experimental and theoretical molecular weights and low dispersities (*Đ* = 1.02). This demonstrates that the supramolecular photocatalyst can significantly accelerate the rate of polymerization while maintaining excellent control even if such DMA polymerizations are conducted in open reactors.

Subsequently, we applied this high-throughput synthesis platform to various alternative monomers, including *N*-acryloylmorpholine (NAM), *N*-(2-hydroxypropyl) methacrylamide (HPMA), and poly(ethylene glycol) methyl ether acrylate (PEGA), poly(ethylene glycol)methyl ether methacrylate (PEGMA) (**Table S8, Figure S20–S21**). Near-quantitative conversions were observed for each monomer except for HPMA, which is a methacrylamide with a relatively low k_p value. GPC analysis indicated good agreement between theoretical and experimental molecular weights and narrow molecular weight distributions; the relatively high dispersity (*Đ* = 1.32) observed for PPEGA is attributed to steric congestion and a chain transfer to polymer side reaction for this acrylate monomer.[23a, 24] In addition, chain extension from a $PDMA_{190}$ precursor (M_n = 19 kg mol^{-1}, *Đ* = 1.04) with a second portion of DMA monomer yielded a homopolymer with a higher molecular weight and low dispersity (M_n = 158 kg mol^{-1}, *Đ* = 1.13). GPC analysis revealed a clear shift to lower elution time with no detectable tailing or shoulder, indicating the absence any unreacted precursor polymer owing to premature termination. These results demonstrate that the polymer chains prepared using this synthesis platform possess excellent chain-end fidelity (**Figure S22**, **Table S9**).

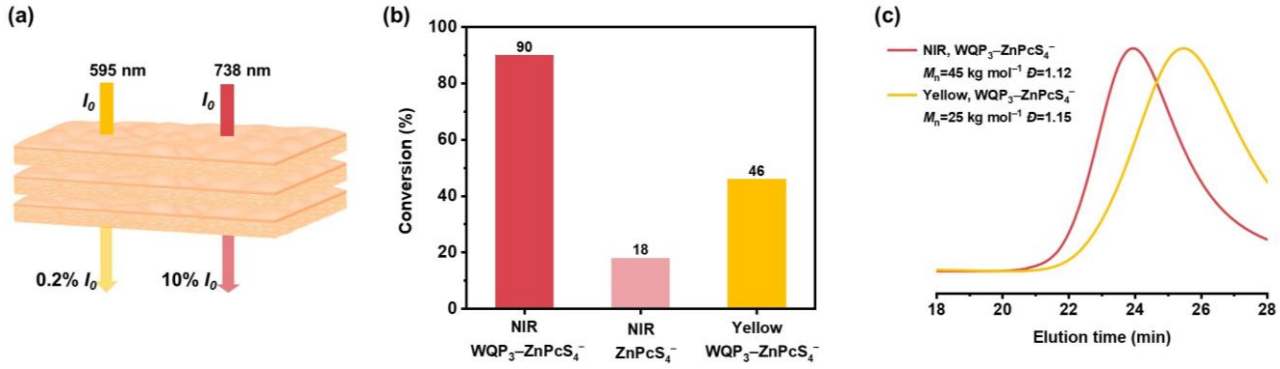

Figure 5. Photopolymerizations conducted through porcine skin. (a) Schematic illustration of the photocontrolled polymerization conducted through three layers of porcine skin (overall skin thickness = 15 mm) under the irradiation of either NIR light (I_0 = 80 mW cm^{-2}, λ_{max} = 738 nm) or yellow light (I_0 = 80 mW cm^{-2}, λ_{max} = 595 nm). (b) Monomer conversions achieved after 14 h. (c) GPC traces recorded for the PDMA homopolymers obtained after the corresponding polymerization. Polymerization conditions: [DMA] = 50% v/v, [DMA]/[CTPA] = 500, [TEOA] = 0.19 M, [$ZnPcS_4^-$] = 0.24 mM (50 ppm relative to DMA), [WQP_3] = 0.72 mM, solution volume = 170 μL, head space volume = 170 μL, 28 °C.

NIR photocontrolled polymerization conducted through porcine skin

To evaluate the potential of this supramolecular NIR photocatalyst for practical bioapplications, polymerizations of DMA were conducted using different light sources at the same light intensity (80 mW cm^{-2}) using porcine skin (5.0 mm) as a physical barrier. When one or two layers of porcine skin were used as the barrier, both NIR (λ_{max} = 738 nm) and yellow (λ_{max} = 595 nm) light irradiation produced relatively high monomer conversions with slightly higher conversions being observed in the former case (**Figure S25**). However, when three layers of porcine skin (overall thickness = 15 mm) were used as a barrier (**Figure 5a)**, the yellow light exhibited extremely low penetration efficiency (0.2%), which was insufficient to drive effective polymerization (only 46 conversion). In contrast, using NIR light led to superior tissue penetration capability, achieving 10% transmittance and 90% conversion, which is markedly higher than that obtained for the equivalent polymerization conducted using $ZnPcS_4^-$ alone (18% conversion, see **Figure 5b**). GPC analysis indicated that a low-dispersity PDMA homopolymer with a predictable molecular weight was still achieved for the NIR-mediated polymerization even in the presence of a thick barrier when the supramolecular photocatalyst was used (**Figure 5c**). These results illustrate the excellent capability of NIR light to penetrate thick biological barriers and further validates the enhanced catalytic performance of the supramolecular complex.

Mechanistic understanding

The photocatalyst $ZnPcS_4^-$ plays dual roles of deoxygenation and polymerization initiation, while its complexation with WQP_3 significantly enhances the polymerization rate and oxygen tolerance. To reveal the effect of host–guest complexation on the reaction kinetics of the key mechanistic steps (**Figure 6a**), we analyzed the consumption of $^3O_2$, the generation of $^1O_2$, and the production of hydroxyl radicals. As monitored using an oxygen optical fiber sensor,[12] the dissolved oxygen was consumed within 40 s when the reaction solution was irradiated with NIR light in the presence of WQP_3–$ZnPcS_4^-$, whereas it took 20 min for a solution

containing $ZnPcS_4^-$ alone to reach a similar oxygen level (**Figure 6b**). This indicates that the supramolecular photocatalyst dramatically accelerates the oxygen photosensitization process. The resulting $^1O_2$ was detected by a spectrophotometric assay using 9,10-anthracenedipropionic acid (ADPA) as a specific probe (**Figure 6c**).[5c] This protocol indicated a significantly faster rate of $^1O_2$ generation for the supramolecular photocatalyst (k = 0.14 min^{-1}) compared to that for $ZnPcS_4^-$ alone (k = 0.06 min^{-1}) (**Figure 6d**). The production of hydroxyl radicals (**Figure S27**) was monitored via electron paramagnetic resonance (EPR) spectroscopy using 2,2,6,6-tetramethylpiperidinooxy (TEMPO) as a radical trap (**Figure 6e**).[25] These experiments showed that the rate of radical trapping was dramatically accelerated in the presence of the supramolecular photocatalyst compared to that when using $ZnPcS_4^-$ alone (reaction rate coefficient, k = 3.51 h^{-1} vs. 0.10 h^{-1}) (**Figure 6f**). This 35-fold increase in reaction rate is attributed to the combined effect of accelerated $^1O_2$ generation and photosensitized H_2O_2 decomposition, thus providing good evidence for the much faster polymerization kinetics in tandem with superior oxygen tolerance.

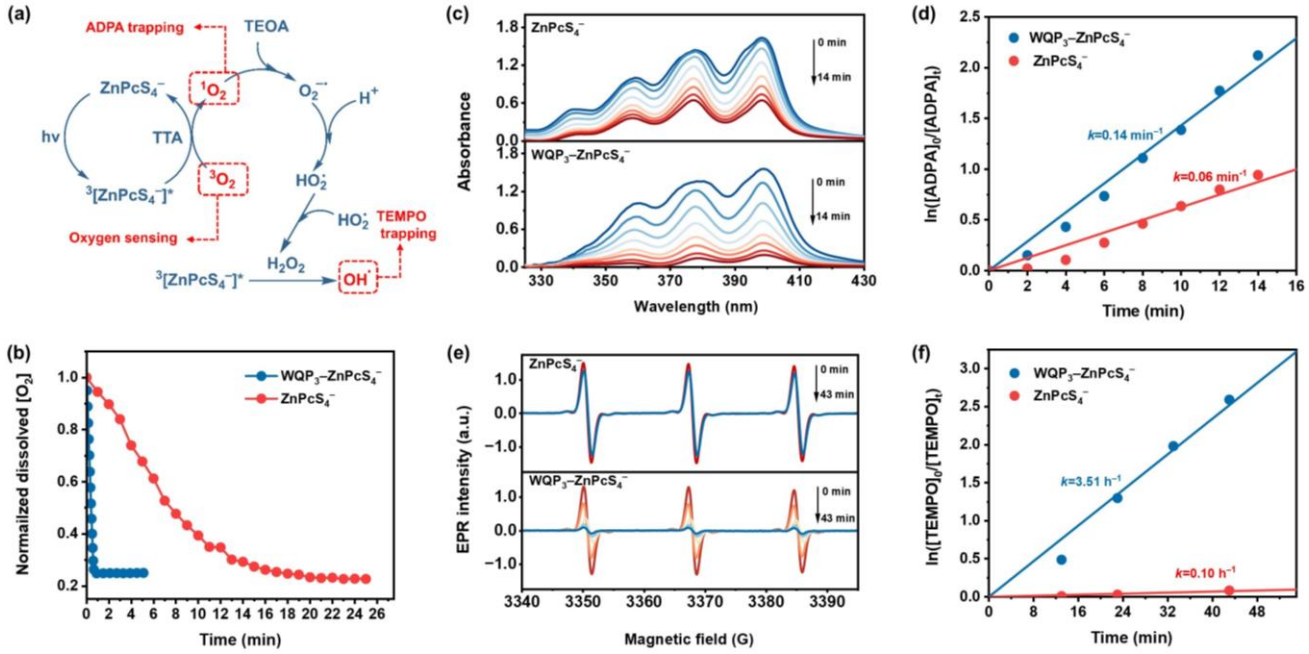

Figure 6. Mechanistic analysis of the superior oxygen tolerance and accelerated kinetics conferred when using the WQP_3–$ZnPcS_4^-$ supramolecular photocatalyst compared to $ZnPcS_4^-$ alone. (a) Proposed NIR photocatalysis-mediated initiation mechanism, with the red color denoting key species for detection. (b) Oxygen consumption measured by an oxygen probe. (c) Spectrophotometric assay for $^1O_2$ formation via ADPA oxidation. (d) Kinetic plots for ADPA oxidation by $^1O_2$. (e) EPR spectra monitoring hydroxyl radical formation via TEMPO trapping. (f) Kinetic plots for hydroxyl radical trapping by TEMPO. Reaction conditions: [TEOA] = 0.19 M, [$ZnPcS_4^-$] = 0.24 mM, [WQP_3] = 0.48 mM, [ADPA] = 0.33 mM, [TEMPO] = 0.50 mM.

Extension to WQP_3–TCPP supramolecular photocatalyst

To demonstrate the modularity and versatility of our new supramolecular approach, we extended the concept to another photocatalyst, tetra(4-carboxyphenyl)porphyrin (TCPP). This metal-free, porphyrin-based compound has been used in the form of particulate aggregates to perform NIR-mediated photoinduced electron transfer-RAFT (PET-RAFT) polymerization in aqueous media.[4j] We hypothesized that transforming such TCPP aggregates into host–guest complexes could significantly enhance its catalytic efficiency and thus enable a faster PET-RAFT polymerization to be achieved even at reduced catalyst loadings.

The disaggregation efficacy of the three biphen[*3*]arenes was evaluated via fluorescence spectroscopy. TCPP has a strong propensity to undergo aggregation in aqueous solution, resulting in pronounced fluorescence quenching.[4j, 26] Gratifyingly, all three macrocycles restored the intrinsic fluorescence of TCPP, with the largest enhancement being observed for WQP_3 (**Figure S29**). This suggests that WQP_3 forms a stable, well-defined host–guest supramolecular complex with TCPP via hydrophobic, π-π, and electrostatic interactions. ^1H NMR spectroscopy studies confirmed inclusion of TCPP within the WQP_3, as evidenced by upfield shifts in proton signals assigned to both TCPP and WQP_3 that simultaneously became broader, owing to the mutal shielding effect between the host and guest molecules (**Figure 7b**). Visible absorption spectroscopy studies indicated the formation of a 1:1 host–guest complex (**Figure 7c–d**). Furthermore, fluorescence titration data (**Figure S30**), ^1H NMR titration experiments (**Figure S33**), and molecular docking studies (**Figure S34**) are consistent

with the formation of a stable, water-soluble WQP_3–TCPP supramolecular complex.

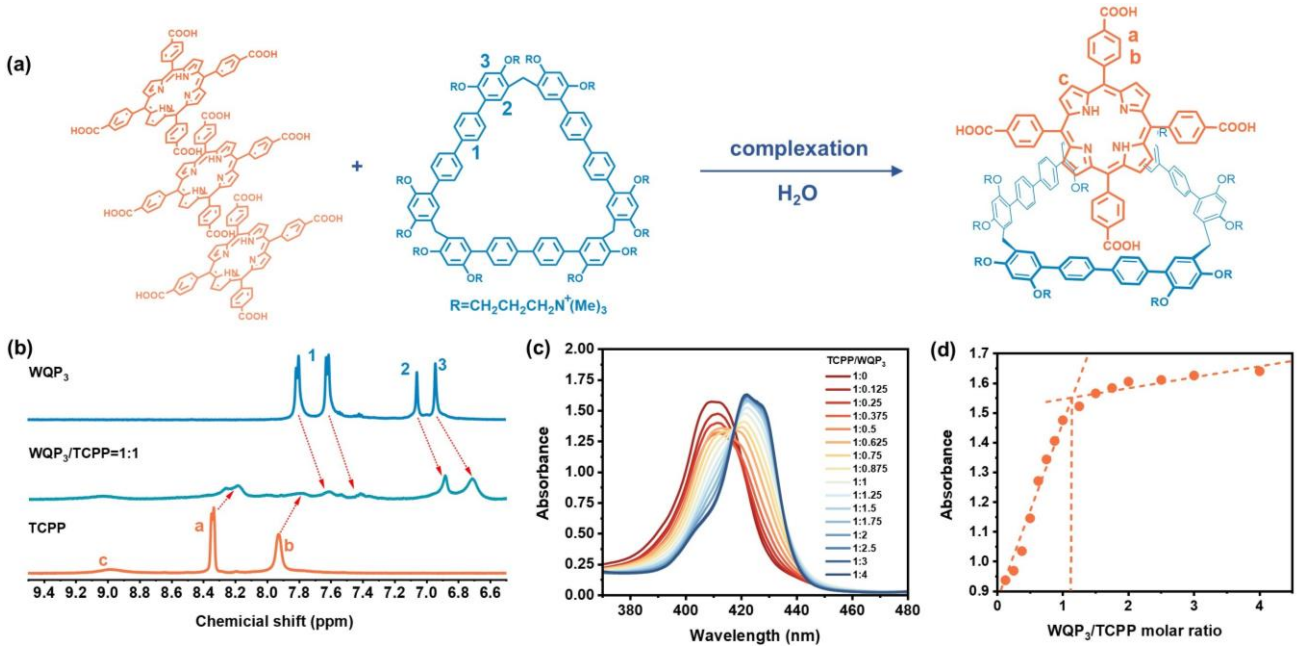

Figure 7. Characterization of host–guest complexation between WQP_3 and TCPP. (a) TCPP alone forms aggregates in aqueous solution but the WQP_3 macrocyclic host binds with TCPP to form a water-soluble supramolecular complex. (b) 500 MHz ^{1}H NMR spectra recorded at 25 °C for WQP_3 (0.8 mM), WQP_3/TCPP = 1:1 (0.8 mM), TCPP (0.8 mM) (PB buffer/DMSO-d_6 = 37:13, 0.2 M) PB buffer prepared in D_2O, pH = 7). (c) Spectrophotometric monitoring of WQP_3 titration into a TCPP solution ([TCPP] = 10 μM). (d) Plots of absorbance at 421 nm versus WQP_3/$ZnPcS_4^-$ molar ratio.

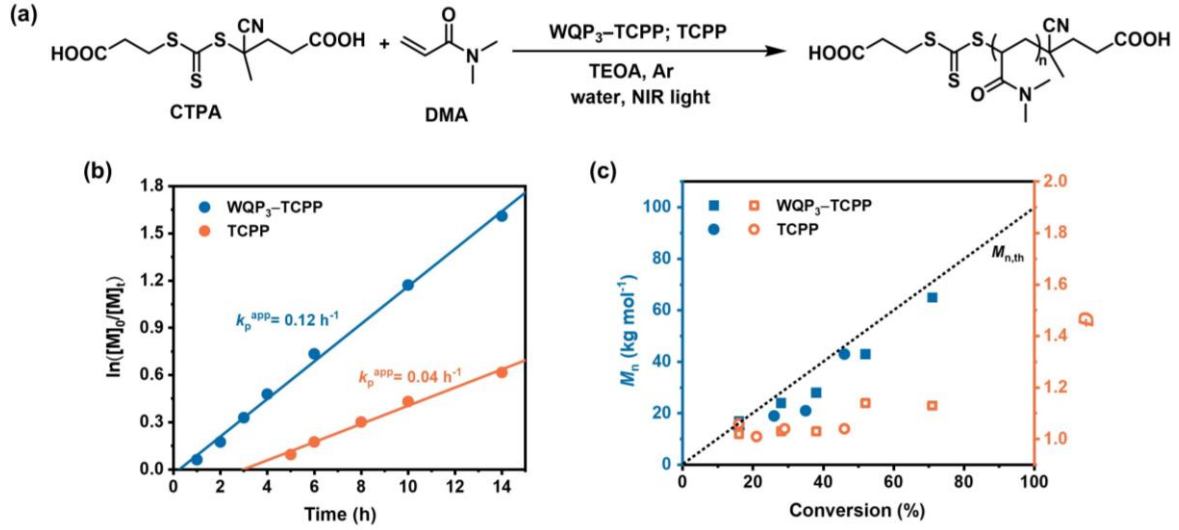

Figure 8. (a) Reaction scheme for DMA polymerization using WQP_3–TCPP or TCPP alone. (b) Pseudo-first-order plots of $\ln([M]_0/[M]_t)$ versus time. (c) Plots of molecular weight and dispersity versus conversion. Polymerization conditions: [DMA] = 30% v/v, [DMA]/[CTPA] = 1000, [TEOA] = 5.82 mM, [TCPP] = 0.29 mM (200 ppm), [WQP_3] = 0.58 mM, solution volume = 1.5 mL, argon atmosphere, 20 °C, NIR light (λ_{max} = 730 nm; I = 120 mW cm^{-2}).

To validate the enhanced catalytic efficacy, we used the WQP_3–TCPP supramolecular photocatalyst to conduct the NIR-mediated PET-RAFT polymerization of DMA in water (**Figure 8a)**. A photocatalytic mechanism using TCPP has been proposed in the literature,[2a] and a similar mechanism is presented in **Figure S35** using the WQP_3–TCPP supramolecular photocatalyst. Again, the WQP_3–TCPP supramolecular photocatalyst exhibited no induction period and faster polymerization kinetics compared to TCPP alone. Importantly, excellent control was retained even at this accelerated polymerization rate as indicated by the pseudo-first-order kinetics, linear increase of M_n with conversion, and narrow molecular weight distributions (**Figure 8**).

Overall, these results demonstrate the modularity and versatility of our new supramolecular strategy for enhancing the performance of NIR photocatalysts.

Conclusion

We have developed a highly effective supramolecular strategy to enhance the performance of NIR photocatalysts for RAFT polymerization in aqueous media. By leveraging the tunable cavity size and cationic functionality of biphen[*3*]arene macrocycles, particularly WQP_3, we constructed well-defined 1:1 host–guest complexes driven by synergistic hydrophobic, π-π, and electrostatic interactions. This supramolecular assembly was confirmed by UV–visible, fluorescence, NMR and ESI-MS studies, as well as GaMD simulations. The resulting WQP_3–$ZnPcS_4^-$ supramolecular photocatalyst enables NIR-mediated RAFT polymerization to be conducted in aqueous solution under ambient conditions with significantly enhanced rates, superior oxygen tolerance, and excellent control over the target molecular weight and dispersity. This polymerization platform is also amenable to high-throughput synthesis in microvolume reactors and retains high efficiency for polymerizations conducted through relatively thick biological barriers. This supramolecular approach is highly modular and can be extended to other photocatalysts such as TCPP, leading to similarly enhanced catalytic performance for RAFT polymerization. This study reports a straightforward and versatile strategy for improving the efficiency of NIR photocontrolled polymerization. Our supramolecular approach not only overcomes the problem of catalyst aggregation but also establishes a robust and oxygen-tolerant platform for precision polymer synthesis under NIR irradiation, thus significantly expanding the toolbox for precison synthesis in the context of both biological and advanced materials applications.

Acknowledgements

We thank the National Key Research and Development Program of China (2021YFA1501600) and the National Natural Science Foundation of China (22371089 , 22193020, and 22193024) for financial support.

Keywords: Supramolecular host–guest complex • near-infrared light photocatalysts • RAFT polymerization • aqueous media

References

[1] a) F. A. Leibfarth, K. M. Mattson, B. P. Fors, H. A. Collins, C. J. Hawker, *Angewandte Chemie International Edition* **2013**, *52*, 199-210; b) M. Chen, M. Zhong, J. A. Johnson, *Chemical Reviews* **2016**, *116*, 10167-10211; c) X. Pan, M. Fantin, F. Yuan, K. Matyjaszewski, *Chemical Society Reviews* **2018**, *47*, 5457-5490; d) C. Aydogan, G. Yilmaz, A. Shegiwal, D. M. Haddleton, Y. Yagci, *Angewandte Chemie International Edition* **2022**, *61*, e202117377; e) S. Zhu, W. Kong, S. Lian, A. Shen, S. P. Armes, Z. An, *Nature Synthesis* **2025**, *4*, 15-30; f) D. A. Corbin, G. M. Miyake, *Chemical Reviews* **2022**, *122*, 1830-1874; g) J. G. Baker, J. Gloriod, C. A. Figg, *Chemical Science* **2025**, *16*, 15298-15309; h) K. Chen, Z. Zhang, Q. Ye, Y. Liu, S. Han, M. Xu, M. Chen, *Chem* **2025**, *11*; i) P. Wen, H. Wang, S. Han, W. Li, L. A. Ah, Z. Zhang, Y. Xu, X. Lin, Y. Shao-Horn, M. Chen, *Joule* **2025**, *9*; j) X.-l. Qin, Z. An, *Acta Polymerica Sinica* **2024**, *55*, 67-78; k) L.-q. Meng, X. Tang, Z. An, *Acta Polymerica Sinica* **2026**, *10.11777/j.issn1000-3304.2026.25326*.

[2] a) Y. Lee, C. Boyer, M. S. Kwon, *Chemical Society Reviews* **2023**, *52*, 3035-3097; b) M. D. Nothling, Q. Fu, A. Reyhani, S. Allison-Logan, K. Jung, J. Zhu, M. Kamigaito, C. Boyer, G. G. Qiao, *Advanced Science* **2020**, *7*, 2001656; c) R. W. Hughes, M. E. Lott, R. A. Olson S, B. S. Sumerlin, *Progress in Polymer Science* **2024**, *156*, 101871; d) M. A. Beres, C. Boyer, M. Hartlieb, D. Konkolewicz, G. G. Qiao, B. S. Sumerlin, S. Perrier, *ACS Polymers Au* **2025**, *5*, 184-213.

[3] D. C. Cabanero, T. Rovis, *Nature Reviews Chemistry* **2025**, *9*, 28-45.

[4] a) Z. Wu, C. Boyer, *Advanced Science* **2023**, *10*, 2304942; b) J. Jiang, G. Ye, F. Lorandi, Z. Liu, Y. Liu, T. Hu, J. Chen, Y. Lu, K. Matyjaszewski, *Angewandte Chemie International Edition* **2019**, *58*, 12096-12101; c) C. Tian, P. Wang, Y. Ni, L. Zhang, Z. Cheng, X. Zhu, *Angewandte Chemie International Edition* **2020**, *59*, 3910-3916; d) C. Kütahya, C. Schmitz, V. Strehmel, Y. Yagci, B. Strehmel, *Angewandte Chemie International Edition* **2018**, *57*, 7898-7902; e) Z. Wu, T. Zhang, X. Shi, N. Corrigan, G. Ng, C. Boyer, *Angewandte Chemie International Edition* **2023**, *62*, e202302451; f) Q. Ti, L. Fang, W. Zhao, L. Bai, H. Zhao, X. Ba, W. Chen, *Journal of the American Chemical Society* **2023**, *145*, 26160-26168; g) H. Zha, L. Cheng, Z. Wang, C. Liu, C. Hong, *Science China Chemistry* **2024**, *67*, 2353-2361; h) X. Hu, R. Yin, J. Jeong, K. Matyjaszewski, *Journal of the American Chemical Society* **2024**, *146*, 13417-13426; i) Z. Liu, X. Hu, L. Luo, G. He, A. Mazumder, E. Gunay, Y. Wang, E. C. Dickey, L. A. Peteanu, K. Matyjaszewski, R. Jin, *Journal of the American Chemical Society* **2025**, *147*, 28241-28250; j) S. Allison-Logan, Q. Fu, Y. Sun, M. Liu, J. Xie, J. Tang, G. G. Qiao, *Angewandte Chemie International Edition* **2020**, *59*, 21392-21396.

[5] a) S. Shanmugam, J. Xu, C. Boyer, *Angewandte Chemie International Edition* **2015**, *55*, 1036-1040; b) Z. Wu, T. Zhang, X. Shi, N. Corrigan, G. Ng, C. Boyer, *Angew Chem Int Ed Engl* **2023**, *62*, e202302451; c) Z. Wu, W. Fang, C. Wu, N. Corrigan, T. Zhang, S. Xu, C. Boyer, *Chemical Science* **2022**, *13*, 11519-11532; d) N. Corrigan, J. Xu, C. Boyer, *Macromolecules* **2016**,

49, 3274-3285; e) Z. Wu, C. Boyer, *Adv Sci (Weinh)* **2023**, *10*, e2304942; f) S. Shanmugam, J. Xu, C. Boyer, *Macromolecules* **2014**, *47*, 4930-4942.
[6] S. Allison‐Logan, Q. Fu, Y. Sun, M. Liu, J. Xie, J. Tang, G. G. Qiao, *Angewandte Chemie International Edition* **2020**, *59*, 21392-21396.
[7] a) C. Wu, K. Jung, Y. Ma, W. Liu, C. Boyer, *Nature Communications* **2021**, *12*, 478; b) Z. Wu, K. Jung, C. Boyer, *Angewandte Chemie International Edition* **2019**, *59*, 2013-2017; c) J. Sun, S. Ren, H. Zhao, S. Zhang, X. Xu, L. Zhang, Z. Cheng, *ACS Macro Letters* **2023**, *12*, 165-171.
[8] Q. Li, Z. Lu, H. Yang, J. Cai, X. Yin, Y. Zhao, L. Xiao, L. Hou, *Polymer Chemistry* **2022**, *13*, 527-535.
[9] L. Trachsel, I. O. Levkovsky, X. Hu, H. Murata, K. Matyjaszewski, *Journal of the American Chemical Society* **2025**, *147*, 32096-32109.
[10] a) P. Wei, X. Yan, F. Huang, *Chemical Society Reviews* **2015**, *44*, 815-832; b) M. Yan, S. Wu, Y. Wang, M. Liang, M. Wang, W. Hu, G. Yu, Z. Mao, F. Huang, J. Zhou, *Advanced Materials* **2024**, *36*, e2304249; c) M. Morimoto, S. M. Bierschenk, K. T. Xia, R. G. Bergman, K. N. Raymond, F. D. Toste, *Nature Catalysis* **2020**, *3*, 969-984; d) B. Tang, J. Zhao, J.-F. Xu, X. Zhang, *Chemistry-a European Journal* **2020**, *26*, 15446-15460; e) Z. Wang, C. Sun, K. Yang, X. Chen, R. Wang, *Angewandte Chemie International Edition* **2022**, *61*, e202206763; f) H. Wu, T. Xia, F. Qi, S. Mei, Y. Xia, J.-F. Xu, X. Zhang, *CCS Chemistry* **2023**, *5*, 823-829; g) J. Yang, Z. Yang, H. Wang, Y. Chang, J.-F. Xu, X. Zhang, *Angewandte Chemie International Edition* **2024**, *63*, e202402291; h) J. Zhao, H. Yu, X. Jin, B. Qin, S. Mei, J.-F. Xu, X. Zhang, *Science* **2024**, *385*, 1354-1359; i) H. Ma, Y. Kang, W. Xu, Y. Shen, H. Yu, H. Hu, X. Tang, J.-F. Xu, X. Zhang, *Angewandte Chemie International Edition* **2025**, *64*, e202505069; j) H. Ma, W. Xu, X. Tang, Y. Kang, J.-F. Xu, X. Zhang, *CCS Chemistry* **2025**, *7*, 832-842; k) W. Xu, Y. Du, H. Ma, X. Tang, Q. Ou, J.-F. Xu, X. Zhang, *Angewandte Chemie International Edition* **2025**, *64*, e202413129.
[11] E. Alarcón, A. M. Edwards, A. M. Garcia, M. Muñoz, A. Aspée, C. D. Borsarelli, E. A. Lissi, *Photochemical & Photobiological Sciences* **2009**, *8*, 255-263.
[12] R. Li, S. Zhang, X. Tang, G. G. Qiao, S. P. Armes, Z. An, *Journal of the American Chemical Society* **2025**, *147*, 33153-33161.
[13] a) H. Chen, J. Fan, X. Hu, J. Ma, S. Wang, J. Li, Y. Yu, X. Jia, C. Li, *Chemical Science* **2015**, *6*, 197-202; b) Z.-Y. Zhang, C. Li, *Accounts of Chemical Research* **2022**, *55*, 916-929; c) K. Xu, Z. Y. Zhang, C. Yu, B. Wang, M. Dong, X. Zeng, R. Gou, L. Cui, C. Li, *Angewandte Chemie International Edition* **2020**, *59*, 7214-7218; d) K. Xu, Z.-Y. Zhang, Z. Zhou, C. Li, *Chinese Chemical Letters* **2022**, *33*, 2451-2454; e) K. Xu, B. Li, S. Yao, Z. Li, Y. Lu, M. Dong, J. Qiu, L. Luo, C. Li, *Angewandte Chemie International Edition* **2022**, *61*, e202203016.
[14] X. N. Sun, A. Liu, K. Xu, Z. Zheng, K. Xu, M. Dong, B. Ding, J. Li, Z. Y. Zhang, C. Li, *Aggregate* **2024**, *5*, e607.
[15] a) M. Dong, W. Qi, G. Sun, K. Xu, Y. Ma, J.-F. Lv, L. Zhao, Z.-Y. Zhang, C. Li, *Organic & Biomolecular Chemistry* **2023**, *21*, 6926-6931; b) Y. Zhao, L. Chen, J. Chen, J. Li, Q. Meng, A. C. H. Sue, C. Li, *Chemical Communications* **2023**, *59*, 5858-5861; c) Z. Liu, H. Chen, L. Guo, X. Sun, Z.-Y. Zhang, J. Chen, M. Dong, C. Li, *Chinese Chemical Letters* **2024**, *35*, 109666; d) Y. Zhang, X. Yu, D. Gao, L. Chen, Z. Zhang, Y. Liu, Z. Zheng, J. Chen, C. Li, Q. Meng, *Journal of Medicinal Chemistry* **2024**, *67*, 10425-10435.
[16] a) Y. Shang, F. Zhang, Z. Wang, H. Luo, H. Liu, J. Lu, Y. Feng, J. Wang, A. Liu, C. Zhang, B. Li, J. Chen, M. Dong, C. Li, *ACS Materials Letters* **2024**, *6*, 4291-4301; b) Y. Shang, Q. Zhu, J. Ding, L. Zhao, F. Zhang, J. Lu, Y. Feng, J. Wang, Z. Liu, M. Kuang, C. Li, *Journal of Controlled Release* **2024**, *369*, 75-87.
[17] a) M. E. Alberto, B. C. De Simone, G. Mazzone, E. Sicilia, N. Russo, *Physical Chemistry Chemical Physics* **2015**, *17*, 23595-23601; b) L. B. Josefsen, R. W. Boyle, *Metal-Based Drugs* **2008**, *2008*, 276109.
[18] X. Tang, J. Qin, W. Xu, J.-F. Xu, X. Zhang, *CCS Chemistry* **2025**, *7*, 2044-2053.
[19] a) A. Hennig, H. Bakirci, W. M. Nau, *Nature Methods* **2007**, *4*, 629-632; b) G. Ghale, W. M. Nau, *Accounts of Chemical Research* **2014**, *47*, 2150-2159; c) R. N. Dsouza, U. Pischel, W. M. Nau, *Chemical Reviews* **2011**, *111*, 7941-7980.
[20] a) Frisch, M. J., Trucks, G. W., Schlegel, H. B., Scuseria, G. E., Robb, M. A., Cheeseman, J. R., Scalmani, G., Barone, V., Petersson, G. A., Nakatsuji, H., Li, X., Caricato, M., Marenich, A. V., Bloino, J., Janesko, B. G., Gomperts, R., Mennucci, B., Hratchian, H. P., Ortiz, J. V., Izmaylov, A. F., Sonnenberg, J. L., Williams, Ding, F., Lipparini, F., Egidi, F., Goings, J., Peng, B., Petrone, A., Henderson, T., Ranasinghe, D., Zakrzewski, V. G., Gao, J., Rega, N., Zheng, G., Liang, W., Hada, M., Ehara, M., Toyota, K., Fukuda, R., Hasegawa, J., Ishida, M., Nakajima, T., Honda, Y., Kitao, O., Nakai, H., Vreven, T., Throssell, K., Montgomery Jr., J. A., Peralta, J. E., Ogliaro, F., Bearpark, M. J., Heyd, J. J., Brothers, E. N., Kudin, K. N., Staroverov, V. N., Keith, T. A., Kobayashi, R., Normand, J., Raghavachari, K., Rendell, A. P., Burant, J. C., Iyengar, S. S., Tomasi, J., Cossi, M., Millam, J. M., Klene, M., Adamo, C., Cammi, R., Ochterski, J. W., Martin, R. L., Morokuma, K., Farkas, O., Foresman, J. B., Fox, D. J., Gaussian 16 Rev. C.01, Wallingford, CT, **2016**; b) Y. Miao, V. A. Feher, J. A. McCammon, *Journal of Chemical Theory and Computation* **2015**, *11*, 3584-3595.
[21] A. J. Z. a. B. L. Iverson, *Journal of the American Chemical Society* **2000**, *122*, 8898-8909.
[22] a) R. Chapman, A. J. Gormley, M. H. Stenzel, M. M. Stevens, *Angewandte Chemie International Edition* **2016**, *55*, 4500-4503; b) R. Li, S. Zhang, Q. Li, G. G. Qiao, Z. An, *Angewandte Chemie International Edition* **2022**, *61*, e202213396; c) W. Kong, Z. An, *CCS Chemistry* **2025**.
[23] a) Y. Zhao, S. Zhang, Z. An, *Angewandte Chemie International Edition* **2025**, *64*, e202421851; b) A. Reyhani, S. Allison-Logan, H. Ranji-Burachaloo, T. G. McKenzie, G. Bryant, G. G. Qiao, *Journal of Polymer Science Part A: Polymer Chemistry*

2019, *57*, 1922-1930.
[24] a) H. Lu, Y. Huang, E. Zhang, Y. Liu, F. Lv, L. Liu, Y. Ma, S. Wang, *ACS Macro Letters* **2021**, *10*, 996-1001; b) Z. Qing, W. Wang, R. Li, Z. An, *Macromolecules* **2025**, *58*, 6771-6780.
[25] S. Lian, S. P. Armes, Z. An, *CCS Chemistry* **2025**, *7*, 2304-2314.
[26] Z. Zhang, Y. Zhu, X. Chen, H. Zhang, J. Wang, *Advanced Materials* **2019**, *31*, e1806626.

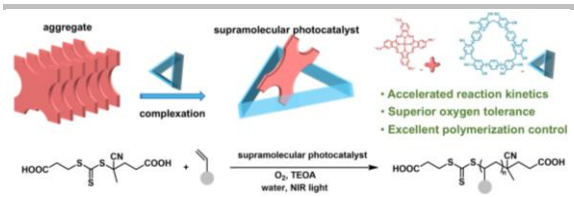

Host–guest supramolecular photocatalysts constructed from NIR photocatalysts and quaterphen[*3*]arenes are developed for RAFT polymerization in aqueous media, resulting in significantly enhanced polymerization efficiency and oxygen tolerance with retained polymerization control.